https://doi.org/10.5194/essd-2022-137
Preprint. Discussion started: 8 June 2022

Open Access Earth System Science Data Discussions

An 8-day composited 36 km SMAP soil moisture dataset from 1979 to 2015 produced using a random forest and historical CCI data

Haoxuan Yang[1], Qunming Wang[1*], Wei Zhao[2], and Peter M. Atkinson[3,4]

[1]College of Surveying and Geo-Informatics, Tongji University, 1239 Siping Road, Shanghai 200092, China.
[2]Institute of Mountain Hazards and Environment, Chinese Academy of Sciences, Chengdu 610041, China.
[3]Faculty of Science and Technology, Lancaster University, Lancaster LA1 4YR, UK.
[4]Geography and Environment, University of Southampton, Highfield, Southampton SO17 1BJ, UK.

Correspondence to: Qunming Wang (wqm11111@126.com)

Abstract. Soil moisture (SM) plays a significant role in many natural and anthropogenic systems which are essential to supporting life on Earth. Thus, accurate measurement and assessment of changes in soil moisture globally is of great value, including long-term historical assessment. Since the on-board cycle and detailed parameters of disparate sensors are different, the European Space Agency established the Climate Change Initiative (CCI) program to harmonize the available multisource SM data, producing long time-series surface SM datasets starting from 1978 to the present. However, the Soil Moisture Active Passive (SMAP) mission, launched in 2015, has shown more satisfactory performance in both spatial accuracy and in capturing pattern of temporal changes. In this paper, a random forest (RF) model was proposed to extend the superior SMAP dataset historically (named RF_SMAP), using the corresponding CCI time-series. We assumed that the temporal changes in the SMAP dataset are similar generally to those in the available CCI dataset. Accordingly, the RF model was constructed using the CCI SM v05.2 data, which was migrated to the prediction of the RF_SMAP dataset. The available *in-situ* SM data and the real SMAP data from 2015 to 2019 were used as references to validate the predicted RF_SMAP data. It was shown that compared with the CCI dataset, the predicted RF_SMAP dataset is closer to the *in-situ* SM data and the real SMAP data. Thus, the RF_SMAP dataset was shown to be a reliable substitute for the historical CCI dataset. The new long time-series RF_SMAP dataset, which will be available to download, will be of great value for a range of research in applications such as climate assessment, agricultural planning, food insecurity monitoring and drought assessment and monitoring.

1. Introduction

Soil moisture (SM) plays a vital role in many fields of earth science. It is a basis of energy exchange between the atmosphere and the land surface (Zhou et al., 2021), and an important consideration in agricultural extensification and intensification to support food security (Acharya et al., 2019; Rigden et al., 2020). Likewise, the monitoring of climate change (Jaeger and Seneviratne, 2010; Guillod et al., 2015) and drought (Zhou et al., 2017; Fang et al., 2021) require the long time-series SM data as a key input for analysis. SM can also affect the evapotranspiration of vegetation, which further influences the terrestrial carbon cycle (Wu et al., 2020; Humphrey et al., 2021). Consequently, the acquisition of high-quality and long time-series SM data is crucial to various applications. Both ground sensor-measured (Larson et al., 2008) and satellite-derived SM data (Beck et al., 2021) are available freely and currently cover the globe. These two types of data have disparate characteristics. Sensor-measured SM data are generally considered as the true SM value at the point scale, as the measurement process is fairly direct. Hence, different measurement networks, which consist of several SM monitoring stations, have been successively installed and used around the world. The International Soil Moisture Network (ISMN) is a key example of *in-situ* data derived from various SM measurement networks for scientific research and applications (Dorigo et al., 2011). However, despite the advantage of direct measurement, the limitation of spatial sparsity is

https://doi.org/10.5194/essd-2022-137
Preprint. Discussion started: 8 June 2022

unavoidable. That is, the measured SM data are provided only at the fixed and limited sensor locations available. In contrast, satellite-derived SM data are spatially continuous in the sense that they provide complete spatial coverage. As a result, satellite-derived SM data have greater application value than sensor-measured SM data, especially across large areas (e.g., at the global or national scale). Over the last few decades, various satellite-derived SM data have been produced with active or passive microwave technology, such as the Advanced Microwave Scanning Radiometer-2 (AMSR2) (Cho et al., 2017; Jin et al., 2018), the Soil Moisture and Ocean Salinity (SMOS) (Kerr et al., 2001; Piles et al., 2011), the Soil Moisture Active Passive (SMAP) (Entekhabi et al., 2010; Chan et al., 2016), the Climate Change Initiative program of the European Space Agency (CCI) (Dorigo et al., 2015; Gruber et al., 2017; Gruber et al., 2019), the Advanced Scatterometer (ASCAT) (Bartalis et al., 2007; Zhang et al., 2021), and the Advanced Microwave Scanning Radiometer onboard the Earth Observing System (AMSR-E) (Njoku et al., 2003; Feng et al., 2017). These platforms update SM data continuously and provide flexible choices for research in related fields, such as hydrology.

There are obvious differences between the aforementioned satellite-derived SM datasets due to their disparate frequencies of the sensors. The L-band (~1.4 GHz) is considered to be more suitable for monitoring surface SM than other frequencies (e.g., C-band or X-band) (Kerr et al., 2001). Moreover, although both the SMOS and SMAP missions carry an L-band sensor for retrieving SM, the temperature brightness observations of SMOS have a larger radiometric error than those of SMAP (De Lannoy et al., 2015). Thus, the SMAP dataset is a more satisfactory a priori choice than the SMOS dataset (Al-Yaari et al., 2017). In recent studies, it has also been found that the SMAP dataset (with a spatial resolution of 36 km) is a preferable choice relative to other satellite-derived SM datasets. Ma et al. (2019) evaluated four SM products (i.e., AMSR2, SMAP, SMOS, and CCI) and found that the SMAP product was superior to other SM products in terms of capturing pattern of temporal changes in SM. Kumar et al. (2018) used information theory-based metrics to demonstrate that the error in SMAP retrievals was the minimum amongst the listed SM datasets (i.e., SMAP, AMSR-E, ASCAT, SMOS, and AMSR2). Furthermore, Kim et al. (2018) claimed that compared to ASCAT and AMSR2, SMAP showed closer relation to the *in-situ* time-series data at the global scale.

In addition to the global assessment, regional assessment, which can describe stability in a specific region and guide further improvement of SM products, also revealed the advantage of SMAP. For example, based on a study in the Huai River Basin, China, Wang et al. (2021) showed that SMAP outperformed SMOS data in both winter (December, January, and February) and summer (June, July, and August). Thus, SMAP can be viewed as one of the optimal SM datasets, currently. However, SMAP is the latest satellite-derived SM data, which began providing effective data from April 2015 (Chan et al., 2018), and approximately six years of data storage is not sufficient to support long time-series studies. That is, historical SMAP data before April 2015 are not available, and have to be replaced by SM data derived from other sensors. However, differences in physical characteristics are unavoidable for SM data derived from various sensors, including sensor properties (Hosseini and McNairn, 2017; El Hajj et al., 2019; Bergstedt et al., 2020), retrieval principles (Njoku et al., 2002; Piles et al., 2009; Das et al., 2014), and the spatial resolution of the SM data (Peng et al., 2017; Li et al., 2018; Abowarda et al., 2021).

Compared with the short temporal span of the SMAP dataset, the CCI dataset (with a spatial resolution of 25 km) has the longest temporal span, which contains approximately 40 years of data from November 1978 to the present, although the first CCI SM dataset was publicly released in 2012 (Dorigo et al., 2017; Dorigo et al., 2015). The enormous number of data in the time-series is conducive for accomplishing dynamic monitoring. Ma et al. (2021) monitored the agricultural drought in Southwest China using the CCI dataset from 1978 to 2016 and found that the duration of drought increased over time. Actually, the CCI dataset was produced by merging SM products collected by various sensors, which synergistically combines the strengths of the individual products (Liu et al., 2012; Liu et al., 2011). To expand the spatial-temporal coverage and maintain the consistency of data in a long time-series, different versions of the CCI dataset were produced continuously by introducing new SM datasets, optimizing the retrieval algorithm, and improving sensor inter-calibration efforts (Dorigo et al., 2017). As one of the newest versions, the CCI v05.2 has been used

https://doi.org/10.5194/essd-2022-137
Preprint. Discussion started: 8 June 2022

Open Access Earth System Science Data Discussions

widely. It needs to be emphasized that the CCI v05.2 version firstly includes the SMAP dataset. In addition, there exist two improvements for the CCI v05.2 version compared with the previous versions, including the inter-calibration of AMSR-2 and the retrieval algorithm of radiometer data (Zhao et al., 2021). Although the CCI dataset harmonizes the multiple-sensor datasets to ensure optimal temporal-spatial coverage and the consistency of the data, its accuracy is inevitably affected by the inherent differences between the observed datasets. Therefore, based on the demonstrated advantage of SMAP and CCI, it is of great interest to restore the historical SMAP data before April 2015 to keep the consistency of the SM characteristics in the temporal domain.

In this paper, we proposed to synthesize a spatially seamless (i.e., 8-day composited) 36 km SMAP dataset at the global scale from January 1979 to March 2015. This was undertaken by transferring the CCI dataset from 1979 to 2015, with a random forest (RF)-based learning model constructed between the CCI dataset before and after April 2015. By assuming that the pattern of temporal changes of the CCI dataset is similar to that of the SMAP data, the trained RF model can be applied to the SMAP data after April 2015, producing the synthesized SMAP dataset before April 2015. For clarity, the synthesized SMAP dataset is denoted as RF_SMAP in this paper. The predicted RF_SMAP dataset retains the advantage of the observed SMAP dataset. Furthermore, since the 8-day composited SMAP dataset after April 2015 is spatially seamless, the RF_SMAP dataset transferred from them is also spatially seamless. This helps to address the gap issues in the CCI dataset. The RF_SMAP dataset can support the use of homologous SM data in long-term series studies without the need for multi-sensor SM data, which can help to avoid the uncertainty introduced by differences between sensors. The predicted historical SMAP data from 1979 to 2015 will be released publicly to support related research based on the need of long time-series SM data at the global scale.

2. Data and methods

2.1. Data description

2.1.1. Satellite sensor data

The 36 km SMAP and 25 km CCI SM dataset used in this paper can be freely collected from the National Snow and Ice Data Center (https://nsidc.org/) and the Climate Change Initiative program of the European Space Agency (http://www.esa-soilmoisture-cci.org/), respectively. The SMAP dataset was collected from April 2015 to December 2019, while the CCI dataset was collected from January 1979 to December 2019. For each type of data, 8-day composited data were considered, which can provide spatially seamless SM at the global scale. To match the spatial resolution of both datasets, the 25 km CCI dataset was degraded to 36 km. **Table 1** lists the details of used SM products.

Table 1. The satellite products of SM used in the study.

Product	Spatial resolution	Data version	Sensors type	Data period (mm-dd-yyyy)
SMAP	36 km	Version 6	Passive	04-15-2015 to 12-31-2019
CCI	25 km	v05.2	Active/passive combined	01-01-1979 to 12-31-2019

2.1.2. *In-situ* SM data

In-situ data are always used as reference data for the validation of SM products (Colliander et al., 2017; Ford and Quiring, 2019), and they can be acquired freely from ISMN (https://ismn.earth/en/) (Dorigo et al., 2021). Since passive radiometers cannot penetrate deeper soil, topsoil moisture (< 0.05 m) retrieved from satellite-derived SM data was used alternatively (Adams et al., 2015; Escorihuela et al., 2010; Raju et al., 1995). That is, all depths of the selected *in-situ* observations were not larger than 0.05 m. For each *in-situ* data point, the 8-day data were averaged to match the temporal resolution of the 8-day composited satellite sensor data.

https://doi.org/10.5194/essd-2022-137
Preprint. Discussion started: 8 June 2022

Open Access Earth System Science Data Discussions

We designed two experiments (denoted as Experiments 1 and 2) using data in different periods to test the effectiveness of the proposed method. Specifically, Experiment 1 used data from 15 April 2016 to 31 December 2019 (denoted as 2016105 to 2019361), and Experiment 2 used data before production of the SMAP dataset (from 1979001 to 2015097). It needs to be stressed that there existed differences in the used *in-situ* data between the two experiments, since the old sensors could be defunct and the new sensors can be installed in other locations in different periods. Figure 1 exhibits the locations of the *in-situ* data in Experiments 1 and 2. Table 2 lists details of the *in-situ* observations.

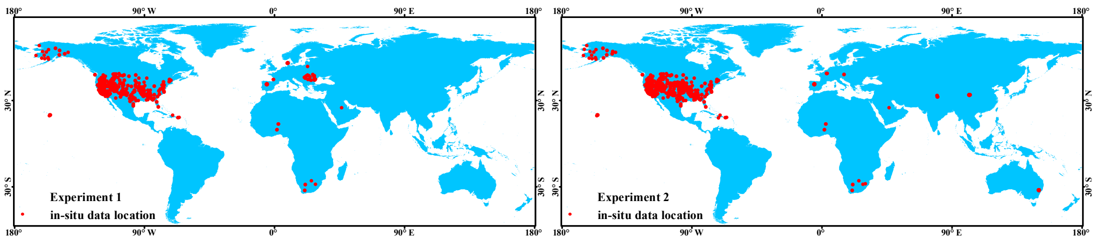

Figure 1. Locations of the *in-situ* data in Experiments 1 and 2.

Table 2. Details of the *in-situ* data used in the experiments.

Experiment	Network	Number of *in-situ* points	Location	Period (Format: YYYYDOY)
	AMMA-CATCH	7	Benin, Niger, Mali	2016105-2018361
	BIEBRZA_S-1	27	Poland	2016105-2018329
	FLUXNET-AMERIFLUX	2	USA	2016105-2019361
	FR_Aqui	3	France	2016105-2019361
1	HOBE	29	Denmark	2016105-2019065
	PBO_H2O	150	USA, Saudi Arabia, South Africa	2016105-2017305
	REMEDHUS	20	Spain	2016153-2019361
	RSMN	20	Romania	2016121-2019361
	SCAN	218	USA	2016105-2019361
	AMMA-CATCH	7	Benin, Niger, Mali	2006001-2015097
	ARM	22	USA	2003001-2013313
	AWDN	49	USA	2002177-2010361
	HOAL	33	Austria	2013201-2015097
	MAQU	27	China	2008169-2014305
2	NGARI	23	China	2011209-2014313
	ORACLE	3	France	1997193-2013241
	PBO_H2O	150	USA, Saudi Arabia, South Africa	2012001-2015097
	REMEDHUS	24	Spain	2005081-2015097
	SASMAS	14	Australia	2006001-2007361
	SCAN	226	USA	1996145-2015097

2.2. The proposed RF model for historical SMAP dataset reconstruction

The RF model is a multiple decision tree-based ensemble method, which can characterize the relation between independent and dependent variables reliably with nonlinear regression (Breiman, 2001; Grimm et al., 2008). For the RF model, a bootstrap-based sampling method was used to select the training samples of each tree (approximately two-thirds of all the inputs) for each tree of the model. The remaining one-third of the inputs did not participate in the training process and acted as out-of-bag (OOB) data to validate the constructed model for each bootstrap-based sampling process (Hu et al., 2020; Meng et al., 2020). In addition, the number of regression trees in the forest (n_tree) was also a vital parameter. Guided by the OOB error, n_tree in this research was set to 200 (Zhao et al., 2018).

https://doi.org/10.5194/essd-2022-137
Preprint. Discussion started: 8 June 2022

Surface SM is affected directly by precipitation, and intra-annual variation in precipitation is closely related to seasonal changes (e.g., for the Southern Hemisphere, the precipitation in winter is less than that in summer). Consequently, it can be assumed that temporal variation in surface SM is associated with seasonal changes. Seasonal change is a periodic process across an entire year that is expected to repeat in subsequent years. Accordingly, the surface SM shows approximate periodic inter-annual variation, exclusive of the occurrence of abnormal climate changes. Therefore, the data selected from an entire year (i.e., 46 scenes of 8-day composited SM data) are assumed to have a complete characterization of the temporal pattern, which can be used as the input of training data.

The full CCI SM dataset is available from January 1979 to December 2019. The relation between the CCI dataset before April 2015 and after that (i.e., from April 2015 to December 2019, the effective collection time of the SMAP data) can be characterized by a learning model based on RF. Specifically, it is expressed explicitly as follows:

$$\mathbf{CCI}_t = f(\mathbf{CCI_1}, \mathbf{CCI_2}, \mathbf{CCI_3} \ldots \mathbf{CCI_{46}}) \tag{1}$$

where $\mathrm{CCI_t}$ is the known CCI SM data (i.e., output of training data) at a time after April 2016 (in Experiment 2) or before April 2015 (in Experiment 1), and $\mathrm{CCI_1}$, $\mathrm{CCI_2}$, $\mathrm{CCI_3}$ … $\mathrm{CCI_{46}}$ are the inputs of training data in an entire year falling within April 2015 to April 2016. The input needs to contain a comprehensive pattern of changes for the pixels. In this paper, the period from April 2015 to April 2016 was considered for two reasons. First, the pattern of changes in SM in each of the five years of SMAP is generally the same. Second, this period is closer to the prediction time (i.e., the time before April 2015).

Although there are inevitable differences between the SMAP and CCI SM data, for each pixel, the temporal variation in SM for the two datasets is similar. We selected randomly six pixels at the global scale to exhibit the pattern of changes in SM in the overlapping period (April 2015 to December 2019). As shown in Figure 2, the values of the two SM datasets are different, but they are similar in general pattern of changes. Based on this similar pattern of changes, we assume that the pattern of changes in CCI SM data can be transferred to SMAP data. Therefore, for a time before April 2015, the prediction of the SMAP dataset (denoted as RF_SMAP dataset) can be viewed as a function (i.e., the operator f characterizing the nonlinear relationship in Eq. (1)) of the inputs of SMAP data. It is notable that the input data for the prediction model needs to be acquired in the same period as that for the training model (i.e., from April 2015 to April 2016). Thus, the RF_SMAP for a time before April 2015 can be predicted based on Eq. (2):

$$\widehat{\mathbf{SMAP}}_t = f(\mathbf{SMAP_1}, \mathbf{SMAP_2}, \mathbf{SMAP_3} \ldots \mathbf{SMAP_{46}}) \tag{2}$$

where $\mathbf{SMAP_1}$, $\mathbf{SMAP_2}$, $\mathbf{SMAP_3}$ … $\mathbf{SMAP_{46}}$ are the input data collected from an entire year (from April 2015 to April 2016) and $\widehat{\mathbf{SMAP}}_t$ is the prediction of SMAP (i.e., the predicted RF_SMAP data). Function f is fitted from the learning model in Eq. (1). The prediction process of the RF_SMAP dataset is shown in Figure 3. For a prediction time t, the specific steps are listed as follows:

(1) To match the spatial resolution of 36 km of the SMAP data, the CCI data were upscaled from 25 km to 36 km by the nearest neighbor method.

(2) All 46 scenes of CCI data from April 2015 to April 2016 (denoted as 2015105 to 2016097) were selected as the input training data, while the known CCI data at the corresponding prediction time t were used as the output.

(3) The selected input and output of training data were used to train the RF model.

(4) The corresponding SMAP data acquired in the overlapping period (i.e., April 2015 to April 2016, or 2015105 to 2016097) were used as the input of the trained RF model. Then, the RF_SMAP dataset at time t can be predicted.

(5) The above steps were repeated for each time in the period from January 1979 to April 2015. Then, the RF_SMAP dataset, as a long time-series, can be acquired.

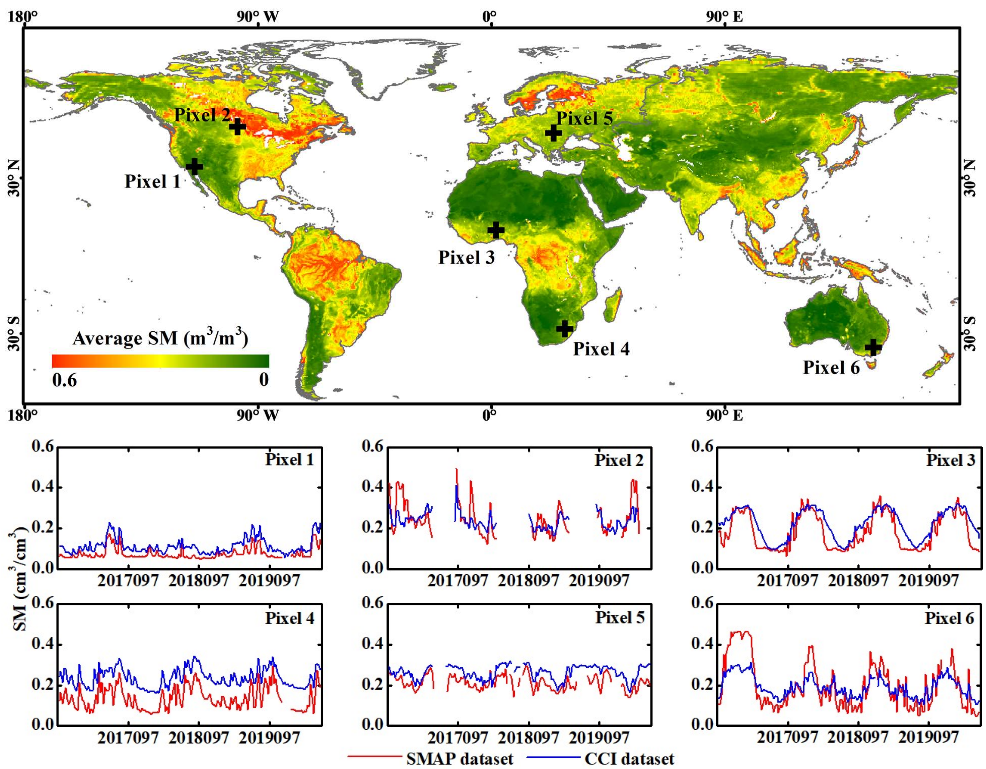

Figure 2. The patterns of changes in SMAP and CCI SM in the overlapping period, where both are available.

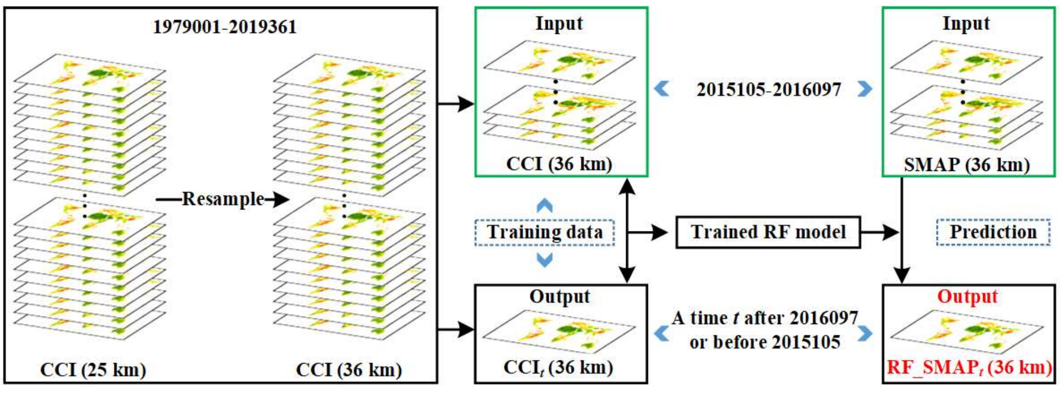

170 **Figure 3. The prediction process of the RF_SMAP dataset on a date before April 2015.**

2.3. Validation method

For Experiment 1, where the SMAP dataset from 15 April 2016 to 31 December 2019 was predicted, the real SMAP dataset is known perfectly. Thus, the SMAP dataset was used for validation of the prediction directly. For both Experiments 1 and 2, the *in-situ* data were also used to validate the predicted RF_SMAP data. The validation was performed separately for each network listed

https://doi.org/10.5194/essd-2022-137
Preprint. Discussion started: 8 June 2022

Open Access Earth System Science Data Discussions

in Table 2. Specifically, each daily *in-situ* data point in each network was averaged to match the 8-day composited SM of SMAP and CCI. Furthermore, the 8-day composited *in-situ* data in each network were averaged to present the data at the network level. Four statistical metrics were used for quantitative evaluation, including the correlation coefficient (CC), root mean square error (RMSE), bias (Bias), and unbiased root mean square error (ubRMSE).

3. Experiments and results

The experimental design is exhibited in Figure 4. Two experiments were performed, which focused on the predictions of the RF_SMAP over the period with true SMAP (April 2016 to December 2019, or 2016105 to 2019361) and the historical period without the SMAP dataset (January 1979 to April 2015, or 1979001 to 2015097).

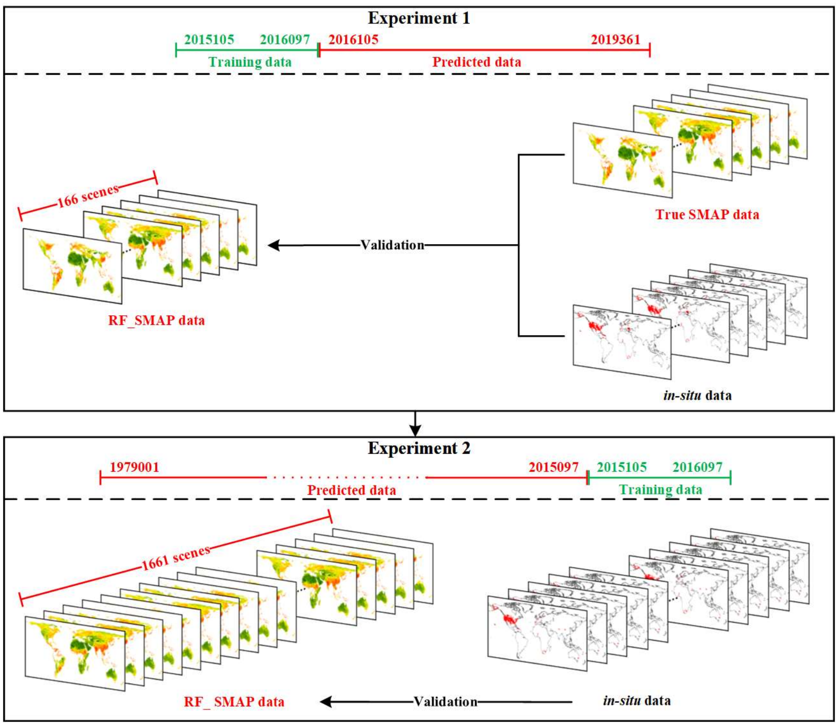

Figure 4. The design for Experiments 1 and 2.

3.1. Experiment 1

We predicted 166 scenes of 8-day composited SMAP data from 2016105 to 2019361. The true SMAP dataset, CCI dataset and the predicted RF_SMAP dataset of four days were selected randomly to exhibit in Figure 5. Three main points can be observed. First, there are noticeable differences between the CCI and true SMAP images. Generally, the CCI SM values range across a smaller interval than that for SMAP. More precisely, for pixels with values very close to the largest value of 0.6 in the SMAP dataset, the corresponding values in the CCI dataset are obviously smaller than 0.6. For pixels with the smallest values (i.e., those close to 0) in the SMAP dataset, the CCI SM values are obviously larger. This conditional bias is mainly attributed to the harmonization process in producing the CCI dataset, which minimizes the difference between the data of various sensors by tuning their values. Second,

https://doi.org/10.5194/essd-2022-137
Preprint. Discussion started: 8 June 2022

compared to the CCI dataset, the predicted RF_SMAP images are much closer to the true SMAP images. The advantage lies in reconstruction of both spatial texture and individual SM values. Specifically, the color of the RF_SMAP images is obviously closer to the SMAP image, and the difference in the texture of some regions is much smaller, such as the orange parts in North America and Asia. Third, the RF_SMAP dataset fills some gaps observed in the CCI dataset. This is because the RF_SMAP dataset is predicted based on the input SMAP dataset collected from April 2015 to April 2016, in which the SMAP data in the corresponding gap areas in CCI are available.

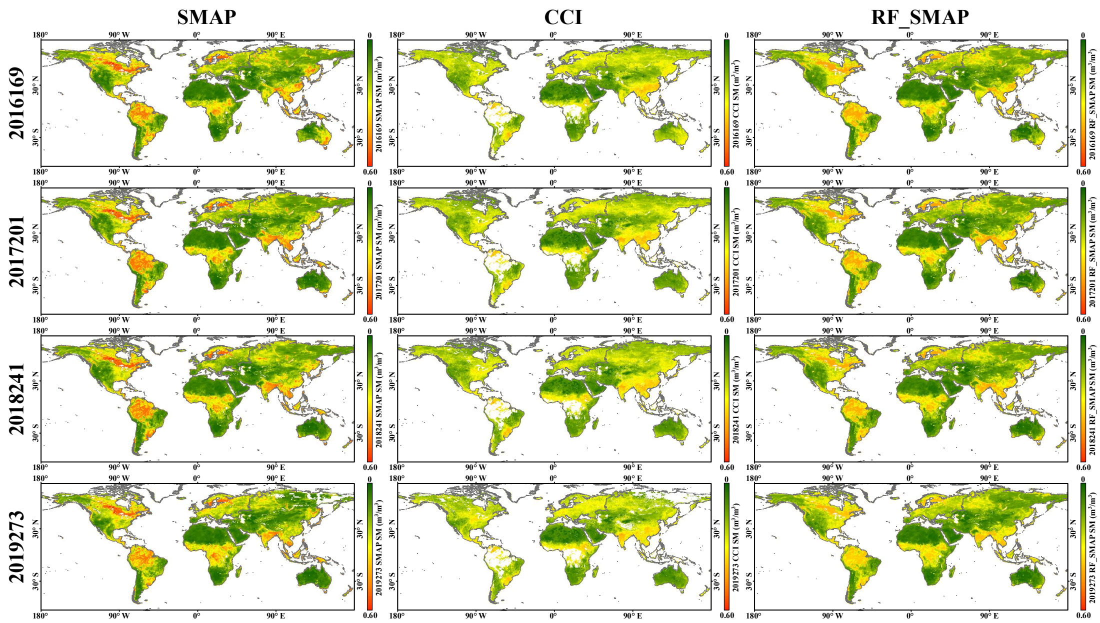

Figure 5. The three satellite-derived SM datasets in Experiment 1

As shown in Figure 6, the true SMAP dataset was used as the reference to evaluate the CCI dataset and RF_SMAP dataset based on the four accuracy metrics. Note that for fair comparison, the common effective part (i.e., without gaps) of the three datasets was considered. It can be seen clearly that the accuracy of RF_SMAP prediction is consistently greater than for CCI on each day. The statistical metrics were averaged from 2016105 to 2019361, and the results are shown in Table 3. The predicted RF_SMAP dataset has an average CC of 0.935, which is 0.198 larger than that for the CCI dataset (with an average CC of 0.737). Both average RMSE and ubRMSE of the RF_SMAP dataset are approximately 0.050 smaller than that of the CCI dataset. The average Bias of RF_SMAP dataset is 0.003, which is also much closer to the reference than that of the CCI dataset (with an average Bias of -0.016).

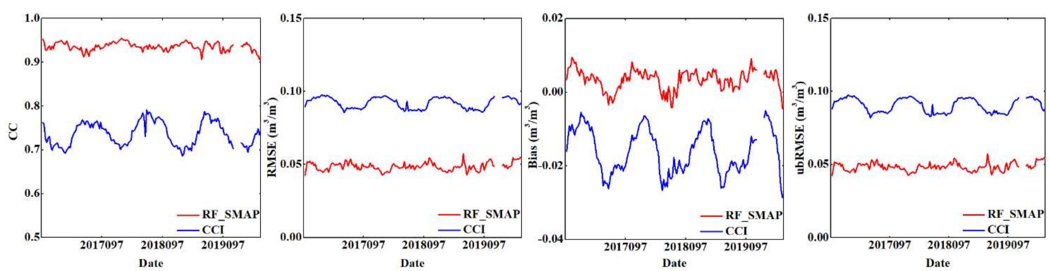

Figure 6. Statistical metrics for accuracy assessment of the CCI and RF_SMAP datasets against the SMAP dataset in Experiment 1.

https://doi.org/10.5194/essd-2022-137
Preprint. Discussion started: 8 June 2022

Table 3. Averaged accuracy indices for all days in Figure 6.

	CC	RMSE	Bias	ubRMSE
RF_SMAP	0.935	0.049	0.003	0.049
CCI	0.737	0.092	-0.016	0.090

The *in-situ* data at the nine networks (see Table 2) were also used to evaluate the observed CCI and the predicted RF_SMAP dataset, as shown in Figure 7. There are some null values in the 8-day composited *in-situ* data, as some of them were not available in the period (not observed by the sensor or acquired with limited quality). It needs to be emphasized that the *in-situ* SM values at the BIEBRZA_S-1 work are larger than those of the corresponding CCI and RF_SMAP datasets and also *in-situ* SM values at other networks. This is because the BIEBRZA_S-1 network is located at a wetland (including grassland and marshland), and the occurrence of floods is common (Dabrowska-Zielinska et al., 2018). Overall, the CCI and RF_SMAP datasets are able to describe the pattern of temporal changes of SM at different locations, which present periodical changes. However, there are noticeable differences between the *in-situ* data and the satellited-derived observations, revealing the inherent uncertainty in satellite-derived observations. Generally, several types of vegetation with different characteristics cover the topsoil, which influence directly the reliability of the SM retrieved from satellite sensor data. Conversely, the *in-situ* data were measured directly from the topsoil, which avoids surface interference.

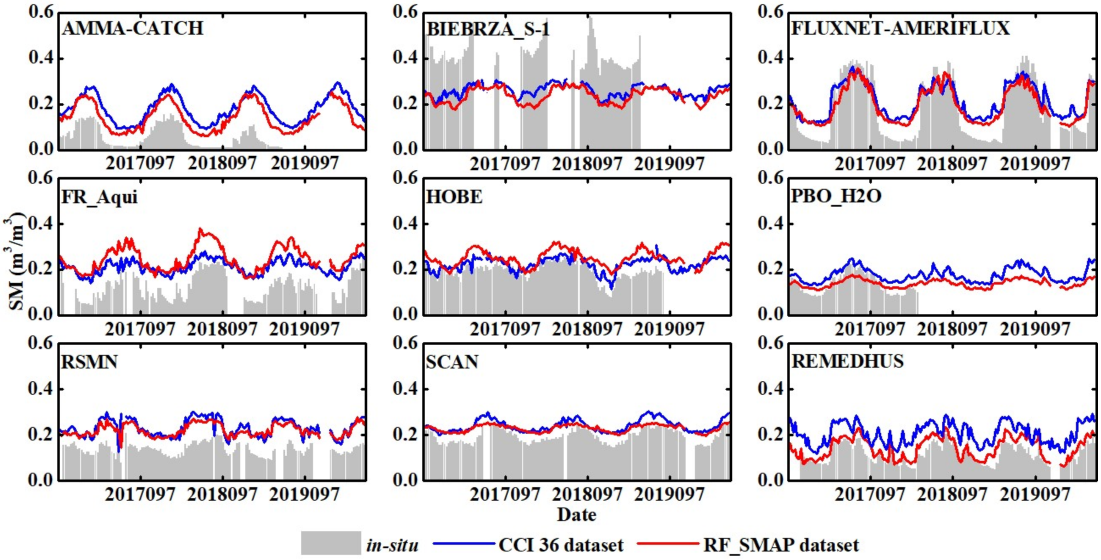

Figure 7. The *in-situ* and the three satellite-derived SM datasets at the nine networks in Experiment 1.

Following Figure 7, the relation in terms of the scatterplots between the CCI or RF_SMAP and the *in-situ* SM datasets is shown in Figure 8. To evaluate directly the accuracies, Table 4 summarizes Figure 8, which lists the four statistical metrics of the CCI and predicted RF_SMAP dataset. The predicted RF_SMAP dataset has an average CC of 0.764, which is 0.015 larger than that of the CCI dataset. The average RMSE of the RF_SMAP dataset is 0.083, which is 0.006 smaller than that of CCI. RF_SMAP and CCI have an average Bias of -0.025 and -0.039, respectively. In addition, the ubRMSEs of the three datasets are similar. Thus, it can be concluded that RF_SMAP is closer to the *in-situ* data than CCI.

AMMA-CATCH **BIEBRZA_S-1** **FLUXNET-AMERIFLUX** **FR_Aqui** **HOBE** **PBO_H2O**

https://doi.org/10.5194/essd-2022-137
Preprint. Discussion started: 8 June 2022

Open Access Earth System Science Data Discussions

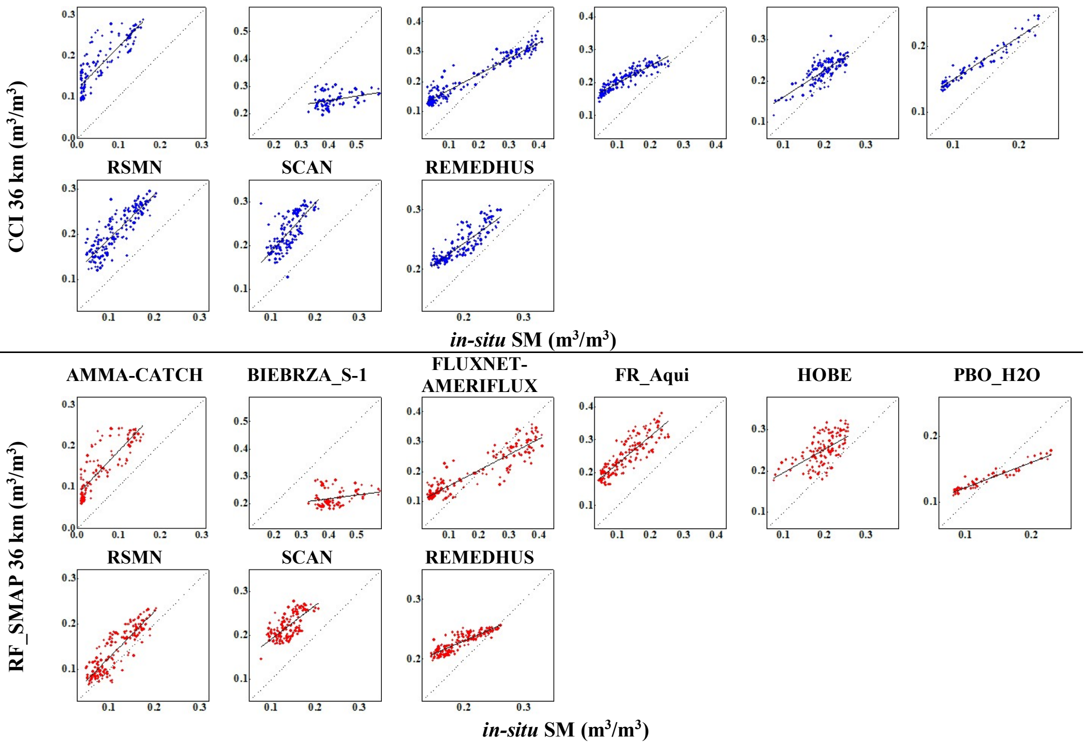

230 **Figure 8. The scatterplots between the *in-situ* data and satellite SM data in Experiment 1.**

Table 4. Statistical metrics for accuracy assessment of the data at each network in Experiment 1 (using the *in-situ* data as reference).

	CC		RMSE (m^3/m^3)		Bias (m^3/m^3)		ubRMSE (m^3/m^3)	
Networks	CCI	RF_SMAP	CCI	RF_SMAP	CCI	RF_SMAP	CCI	RF_SMAP
AMMA-CATCH	**0.847**	0.845	0.126	**0.093**	-0.122	**-0.087**	**0.032**	0.033
BIEBRZA_S-1	0.222	**0.253**	**0.183**	0.207	**0.172**	0.199	0.063	**0.060**
FLUXNET-AMERIFLUX	**0.963**	0.925	0.075	**0.072**	-0.033	**-0.014**	**0.067**	0.071
FR_Aqui	**0.909**	0.867	**0.092**	0.127	**-0.086**	-0.124	0.031	**0.030**
HOBE	0.473	**0.589**	**0.050**	0.064	**-0.021**	-0.055	0.046	**0.033**
PBO_H2O	0.906	**0.967**	0.041	**0.029**	-0.037	**0.000**	**0.018**	0.029
RSMN	**0.703**	0.690	0.096	**0.085**	-0.092	**-0.083**	0.028	**0.021**
SCAN	0.859	**0.861**	0.048	**0.039**	-0.045	**-0.034**	**0.016**	0.020
REMEDHUS	0.862	**0.875**	0.093	**0.035**	-0.090	**-0.026**	0.024	**0.024**
Average	0.749	**0.764**	0.089	**0.083**	-0.039	**-0.025**	0.036	**0.035**

3.2. Experiment 2

In Experiment 2, the historical SMAP dataset from 1979001 to 2015097 was recovered by the proposed RF model. We predicted 1661 scenes of the RF_SMAP dataset, and eight scenes of data could not be predicted due to the absence of the CCI dataset (i.e., dataset on 1981273, 1983273, 1984225, 1986089, 1986097, 1987345, 1987353, and 1988001). As shown in Figure 9, CCI and RF_SMAP datasets on five days were selected randomly for visual comparison. It should be noted that although the 8-day composited CCI dataset was used in this research, many stripe gaps are observed from the earlier CCI dataset (before September 1987). This is because the stripe gaps were produced by the short swath width of the Nimbus7 SMMR radiometer (i.e., 780 km)

https://doi.org/10.5194/essd-2022-137
Preprint. Discussion started: 8 June 2022

(Owe et al., 2008). Additionally, the operation of a single radiometer without the aid of other ones is another reason. After September 1987, numerous stripe gaps were gradually filled with the longer swath width and the appearance of more sensors (Dorigo et al., 2017; Dorigo et al., 2015). Actually, the predicted RF_SMAP dataset accomplishes a more complete spatial coverage based on the corresponding available data in the input SMAP dataset collected from April 2015 to April 2016.

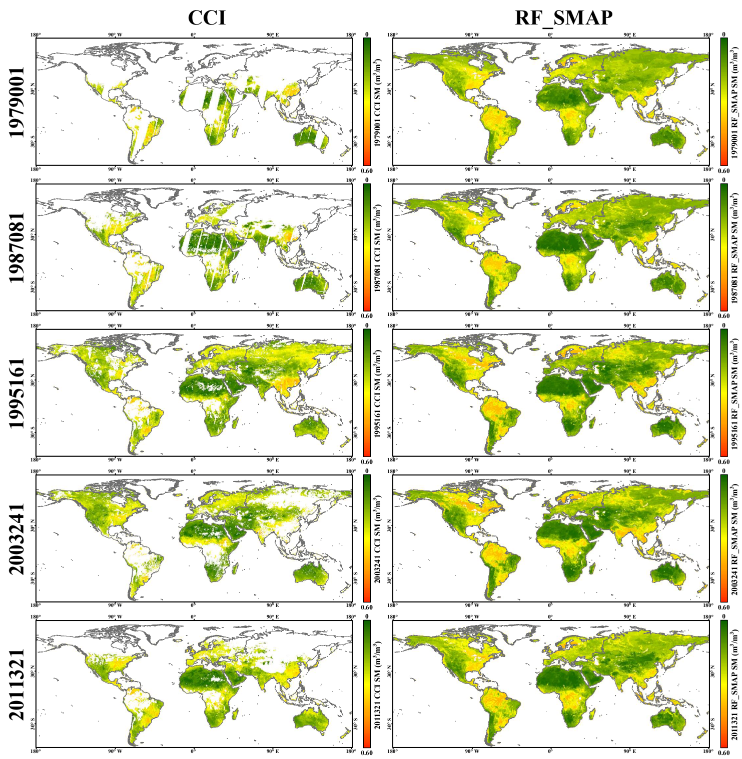

Figure 9. The original CCI and predicted RF_SMAP SM data in Experiment 2.

To compare the accuracy of the CCI dataset and predicted RF_SMAP dataset, the *in-situ* data at 11 networks were used for accuracy assessment, as shown in Figure 10. Both the CCI dataset and predicted RF_SMAP dataset can describe clearly the historical changes and pattern of temporal changes in SM. It needs to be highlighted that the displayed period is different for each network, as these networks have different on-board periods for acquiring data. Thus, the exhibited periods for the satellite-derived SM data need to match the on-board periods of these networks. In addition, the spatial gaps of the CCI data cause interruptions in the CCI time-series for MAQU, NGARI, and HOAL. In contrast, the RF_SMAP dataset generally has a more continuous profile.

https://doi.org/10.5194/essd-2022-137
Preprint. Discussion started: 8 June 2022

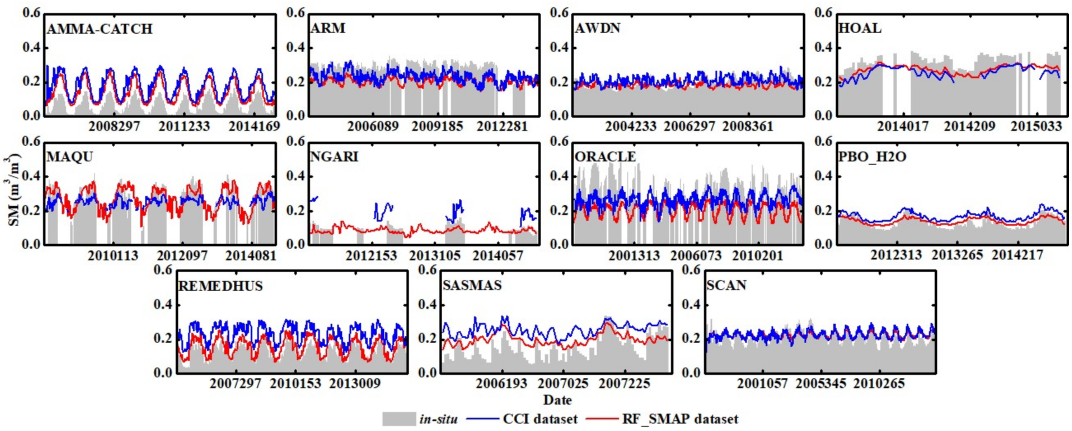

Figure 10. The *in-situ*, CCI and RF_SMAP SM datasets at the 11 networks in Experiment 2.

The scatterplots between the *in-situ* data and the CCI or RF_SMAP dataset are exhibited in Figure 11. The corresponding statistical accuracies are listed in Table 5. We found that the RF_SMAP dataset is more accurate than the CCI dataset based on the four statistical metrics. The RF_SMAP dataset has an average CC of 0.653, which is 0.021 larger than that of the CCI dataset. Moreover, the average RMSE and ubRMSE of the RF_SMAP dataset are 0.025 and 0.014 smaller than those of the CCI dataset, respectively. In addition, the average Bias of RF_SMAP is 0.009, which is closer to the *in-situ* data than that of the CCI dataset

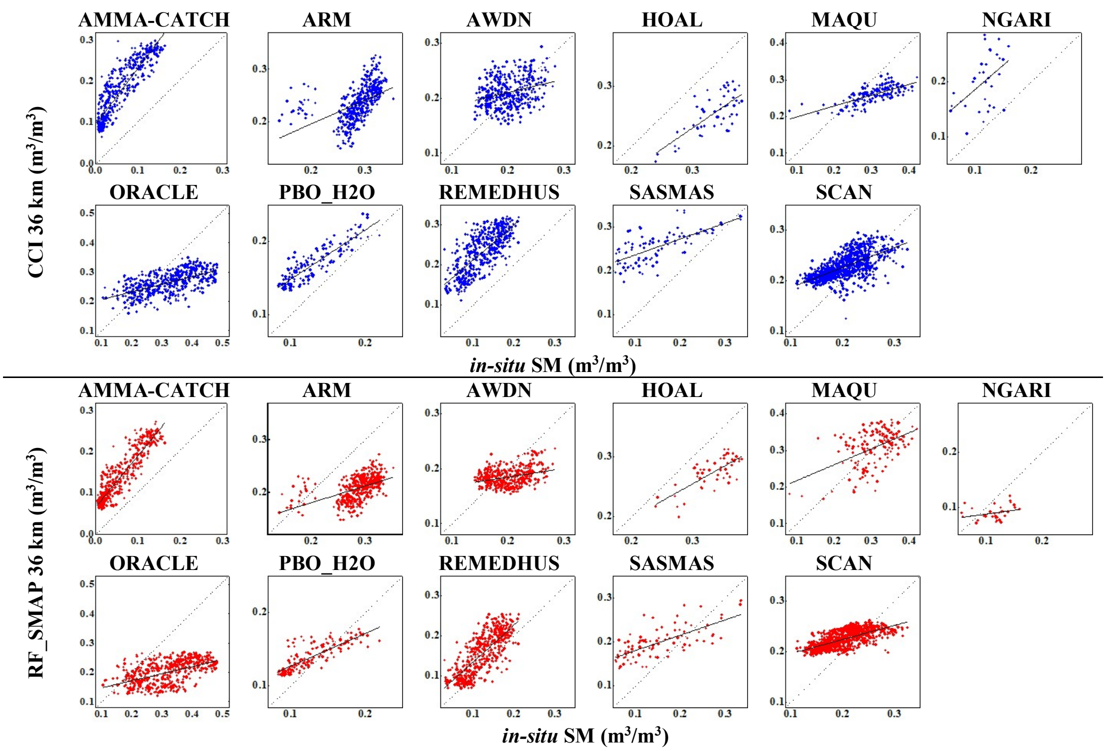

Figure 11. The scatterplots between the *in-situ* data and satellite SM data in Experiment 2.

Table 5. Statistical metrics for accuracy assessment of the data at each network in Experiment 2 (using the *in-situ* data as reference).

	CC		RMSE (m^3/m^3)		Bias (m^3/m^3)		ubRMSE (m^3/m^3)	
Networks	CCI	RF_SMAP	CCI	RF_SMAP	CCI	RF_SMAP	CCI	RF_SMAP
AMMA-CATCH	0.898	**0.923**	0.124	**0.086**	-0.119	**-0.082**	0.035	**0.027**
ARM	0.487	**0.493**	**0.062**	0.085	**0.051**	0.079	0.035	**0.031**
AWDN	0.298	**0.320**	0.036	**0.035**	**-0.010**	0.016	0.035	**0.031**
HOAL	0.627	**0.738**	0.134	**0.063**	0.109	**0.058**	0.077	**0.026**
MAQU	**0.686**	0.645	0.077	**0.052**	0.056	**0.002**	0.053	**0.052**
NGARI	**0.623**	0.544	0.093	**0.029**	**-0.005**	0.022	0.093	**0.019**
ORACLE	0.371	**0.527**	**0.108**	0.140	**0.066**	0.119	0.086	**0.073**
PBO_H2O	**0.890**	0.817	0.042	**0.024**	-0.038	**-0.010**	**0.016**	0.022
REMEDHUS	0.727	**0.773**	0.115	**0.047**	-0.109	**-0.033**	0.036	**0.033**
SASMAS	0.704	**0.714**	0.115	**0.070**	-0.102	**-0.045**	0.053	0.053
SCAN	0.644	**0.682**	0.039	**0.038**	-0.024	**-0.021**	**0.031**	0.032
Average	0.632	**0.653**	0.086	**0.061**	-0.011	**0.009**	0.050	**0.036**

3.3. The influence of the volume of input data in the RF model

Both SMAP and CCI have approximately 210 scenes of SM data during the overlapping period. It means that the maximum number of images that can be used in the input of the RF model is 210. To analyze the influence of the number of data used in the input, we examined the accuracy of the RF model under various numbers of input images. Specifically, the SMAP data on 2019361 were predicted. The initial input of training data includes the earliest 10 known CCI SM images (i.e., from 2015105 to 2015177). Then, the input of training data maintained the existing data and was gradually increased with a step of 10 scenes of CCI SM data, reaching 210 scenes finally. Different RF models were constructed based on the various numbers of inputs (i.e., from 10 to 210 scenes of CCI data). It needs to be emphasized that the inputs of the predicting data (i.e., SMAP data) also changed with the training data (i.e., CCI data). That is, the correspondence in acquisition time between the inputs of training and testing data was maintained consistently. The true SMAP data on 2019361 were used as reference for evaluation. The accuracies under different cases are shown in Figure 12. It can be seen clearly from the four statistical metrics that the accuracy increases remarkably when the number of input images increases from 10 to 40, and becomes stable when the number reaches 40 (the position is indicated by the blue line in Figure 12). In addition, we also investigated the corresponding running time of the RF models. We found that the running time increases linearly when the number of inputs is increased. Obviously, it is not an optimal choice to spend more running time on predicting the RF_SMAP data with similar accuracy. On the other hand, the number of 40 approximates the choice of 46 used in this paper, which covers a full year of data with complete pattern of temporal changes in a cycle. Thus, we determined 46 scenes as the optimal number of input images in the RF model.

https://doi.org/10.5194/essd-2022-137
Preprint. Discussion started: 8 June 2022

Open Access Earth System Science Data Discussions

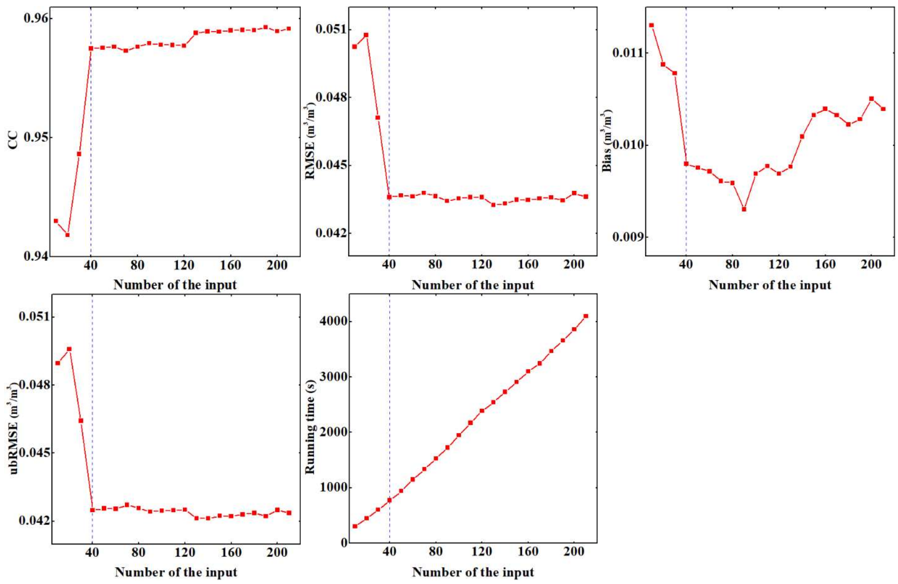

Figure 12. The accuracy under various numbers of the input in the RF model.

3.4. The influence of the solution to the input construction in the RF model

We used the confirmed number of inputs (i.e., 46 scenes of CCI data) to test the input construction method in the RF model. Two input construction methods, called fixed-based and dynamic-based here, were compared. For the fixed-based method, the 46 earliest scenes of the CCI dataset in the overlapping period (i.e., from 2015105 to 2016097) were selected as the fixed input of training data, For the dynamic-based method, the 46 earliest scenes of CCI and SMAP were selected as the initial inputs of training and testing data. Then, for the first prediction date, the SMAP data were predicted using the RF model fitted from the first training process. For the second prediction date, the previous SMAP prediction was used to replace the earliest data (i.e., from 2015105 to 2016097 in the first training process) in the initial input of testing data. This process was repeated along the time line. Accordingly, the input of CCI in the training data was also updated using the observed CCI data in the period.

The two input construction methods were adopted to predict the SMAP data from 2016105 to 2019361. The corresponding true SMAP data were used as the reference to validate the prediction, and the accuracies are. shown in Figure 13. Overall, the fixed-based method was found to be more accurate than the dynamic-based method based on the four statistical metrics. Moreover, we found that the fixed-based method was more stable than the dynamic-based method. Therefore, the fixed-based method is suggested in the proposed RF model.

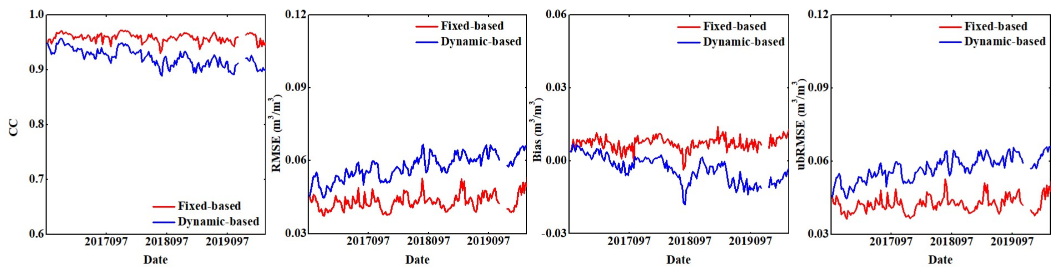

Figure 13. The accuracies of two input construction schemes in the RF model.

https://doi.org/10.5194/essd-2022-137
Preprint. Discussion started: 8 June 2022

Open Access Earth System Science Data Discussions

4. Discussion

4.1. The advantage of the RF model in terms of producing seamless SM data

McNally et al. (2016) pointed out that the spatial coverage of the CCI SM data in eastern Africa was generally limited prior to 1992, presenting noticeable gaps in the CCI SM images. Although with the development of sensor technologies, the spatial coverage of the CCI dataset has increased gradually, there are still gaps in parts of central Africa and northern South America and several other regions, as shown in the left column of Figure 14. Hence, the quality of the historical CCI dataset has always been constrained by this problem, which will affect greatly the reliable analysis of SM at the global scale. However, this problem is alleviated remarkably in the RF_SMAP dataset. As shown in Figure 14, the spatial coverage (e.g., the regions in the blue ellipses) in Africa and South America for the RF_SMAP dataset is generally complete. This can be attributed mainly to the spatially complete coverage of the observed SMAP dataset in the overlapping period of April 2015 to April 2016. Specifically, based on the RF model, the nonlinear relationship between the data before April 2015 and the data within April 2015 to April 2016 is constructed by the known CCI data in this period, and is migrated to the matched input of testing data (i.e., SMAP dataset). As the 8-day composited SMAP dataset is generally seamless, the RF_SMAP data can also be predicted with seamless spatial coverage. This is an important advantage of the proposed RF model.

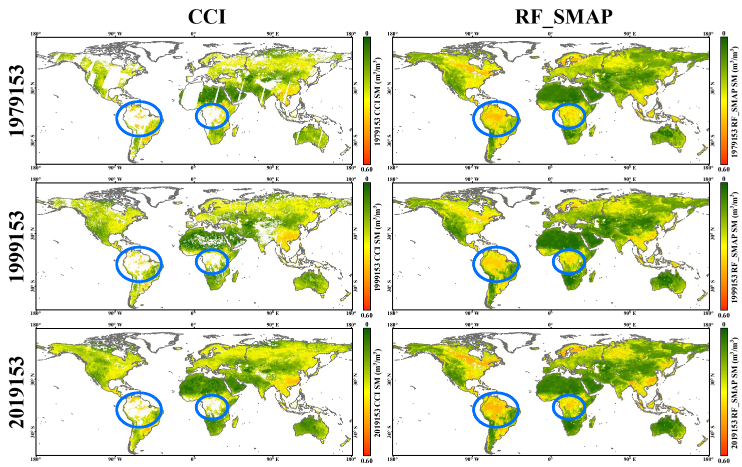

Figure 14. The spatial coverage of the CCI SM and RF_SMAP dataset (the regions in the blue ellipses indicate the areas with gaps in the CCI dataset but complete spatial coverage in the RF_SMAP dataset).

4.2. Monthly changes in global average SM

To evaluate the monitoring capacity of the predicted RF_SMAP data, the monthly change in global average SM was calculated for the three SM datasets (i.e., SMAP, CCI, and RF_SMAP) in the overlapping period (i.e., 2016105 to 2019361), as shown in Figure 15. It is clearly illustrated that the pattern of monthly changes in the RF_SMAP dataset is more similar to the SMAP dataset than the CCI dataset. Table 5 lists the quantitative evaluation for CCI and RF_SMAP datasets, where the SMAP dataset was used as a reference. The RF_SMAP dataset has a CC of 0.971, which is 0.069 larger than that of the CCI dataset. Furthermore, the RF_SMAP dataset has a RMSE of 0.004 and an ubRMSE of 0.003, which is 0.013 and 0.003 smaller than that of the CCI dataset, respectively. In addition, the Bias of the RF_SMAP dataset is 0.003, which is closer to the reference than that of the CCI dataset (with a Bias value of -0.016). It should be emphasized that for fairness, the common effective part of the three datasets was used to calculate the global average SM.

https://doi.org/10.5194/essd-2022-137
Preprint. Discussion started: 8 June 2022

Obviously, the average SM increases from May and reaches its peak in July. Then, the average SM begins to decrease and reaches a previous level around September. This phenomenon is caused by seasonal changes in precipitation; accordingly, the pattern of changes in average SM is similar to that of the average precipitation at the global scale (Konapala et al., 2020; Pascolini-Campbell et al., 2021; Wood et al., 2015). Meanwhile, both the SMAP and RF_SMAP datasets describe the seasonal changes in SM. On the whole, although the SMAP SM values are slightly larger than the CCI and RF_SMAP SM values, the RF_SMAP dataset can still replace the SMAP dataset to explain the periodic changes in SM, which can be a more appropriate choice than the CCI dataset.

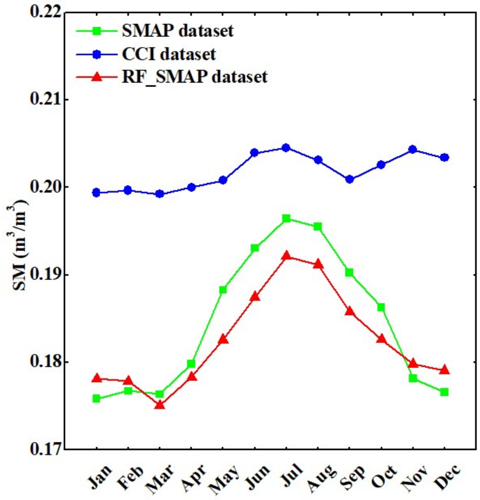

Figure 15. Monthly changes in the global average SM for the SMAP, CCI, and RF_SMAP datasets (calculated based on data from 2016105 to 2019361).

Table 6. Statistical metrics for the monthly changes in SM for the CCI and RF_SMAP datasets (SMAP as reference).

	CCI	RF_SMAP
CC	0.902	0.971
RMSE (m^3/m^3)	0.017	0.004
Bias (m^3/m^3)	-0.016	0.003
ubRMSE (m^3/m^3)	0.006	0.003

4.3. Average SM for different continents

Each continent has different climatic types and patterns of precipitation. The RF_SMAP dataset can be used to calculate integrally the differences in SM between the continents without the interference of spatial gaps. Therefore, as shown in Figure 16a, we calculated the annual average SM of different continents using the RF_SMAP dataset from 1979 to 2015 to compare each continent. In addition, the average for all 36 years was also provided in Figure 16b. From Figure 16a, we can see that the annual SM for all continents in the 36 years is generally stable. As shown in Figure 16b, South America (SA) has the largest average SM of 0.256 (m^3/m^3) among the six continents. The average SM in Europe (EU) and North America (NA) is similar and slightly smaller than that in South America. The average SM in Asia (AS) is the fourth largest, with a value of 0.189 (m^3/m^3), which is 0.036 larger than that in Africa (AF). Oceania (OA, mainland Australia) has the smallest average SM of 0.126 (m^3/m^3).

https://doi.org/10.5194/essd-2022-137
Preprint. Discussion started: 8 June 2022

Open Access Earth System Science Data Discussions

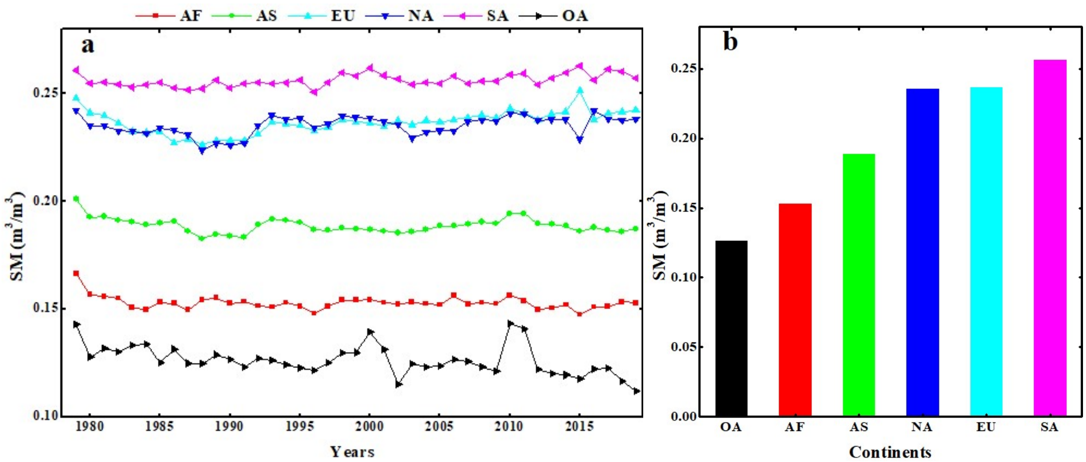

Figure 16. Average SM (from 1979 to 2015) in the six continents.

4.4. The uncertainty in the prediction process

There are two unavoidable uncertainties in the prediction process. First, the RF-based learning model was constructed using the CCI datasets with spatial gaps. The uncertainty in the prediction process is especially large for areas where the CCI data are not available, as the SMAP data were predicted mainly by referring to a relation fitted using CCI data in other areas (e.g., the spatial texture there varies greatly from the gap areas). This issue is prominent when the size of gap is large, where the number of effective training data is also reduced. Second, the RF model is applied based on the assumption that the fitted relationship between the CCI data before April 2015 and the CCI data within April 2015 to April 2016 can be migrated to that for the SMAP data. This is supported by the similar pattern of temporal changes of the CCI and SMAP data (as illustrated in Figure 2) as well as the experimental validation. However, it should be pointed out that the relation fitted using the CCI data may not be perfect for SMAP, considering the obvious differences between the two types of data. Although the proposed RF model has been demonstrated to be an effective solution for creating long time-series SMAP data before April 2015, more efforts are still encouraged to further enhance the accuracy of the predictions in future research. For example, it may be interesting to develop models to construct the relationship between overlapping CCI and SMAP data, but how to fully account for the information in the CCI and SMAP time-series would be an important issue. It would also be important to make fuller use of the available spatial texture information. That is, the spatial content information (e.g., neighborhood information) can be considered in the input construction in the learning model.

5. Conclusion

In this paper, we predicted global 36 km, 8-day composited SM data from 1979 to 2015 based on the development of RF models. We assumed that the CCI dataset has a similar pattern of temporal changes to that of the SMAP dataset. In total, 46 scenes of CCI data acquired from April 2015 to April 2016 were used as the input training data in the RF model. The nonlinear relationships constructed from the CCI dataset were migrated to the SMAP dataset. Based on the fitted RF model and the input of corresponding 46 scenes of SMAP data from April 2015 to April 2016, the SMAP data between 1979 to 2015 were predicted. Disparate networks of *in-situ* data were used to validate the RF model as well as the predicted RF_SMAP data. The experimental results showed that the predicted RF_SMAP dataset maintained the advantage of the SMAP dataset in terms of spatial accuracy and characterizing pattern of temporal changes. More importantly, the RF_SMAP dataset enlarges the temporal span of current SMAP observations to

https://doi.org/10.5194/essd-2022-137
Preprint. Discussion started: 8 June 2022

the same as that of the long time-series CCI SM dataset (i.e., from 1979 to 2015). Furthermore, compared with the CCI SM dataset with many spatial gaps, the predicted RF_SMAP dataset is spatially more complete. Therefore, we conclude that the predicted RF_SMAP dataset is a reliable substitute for the CCI SM dataset. The RF_SMAP dataset will be available at https://doi.org/10.6084/m9.figshare.17621765 to facilitate free usage of the data.

Data availability

The constructed CCI-based training dataset and predicted RF_SMAP dataset are available at https://doi.org/10.6084/m9.figshare.17621765 (Yang et al., 2021).

Author contributions

HY designed the research, analyzed the data, wrote the original manuscript, and produced the dataset. QW revised the whole manuscript and provided the funding to support the research. WZ and PMA provided direction and comments. All authors edited and approved the final manuscript.

Competing interests

The authors declare that they have no conflict of interest.

Acknowledgment

The authors like to thank the NSIDC, Global Energy and Water Cycle Experiment (GEWEX), and European Space Agency (ESA) for making the SMAP, CCI and ISMN data freely available.

Financial support

This research was supported by the National Natural Science Foundation of China under Grants 42171345 and 41971297, and Tongji University under Grant 02502350047.

References

Abowarda, A.S., Bai, L., Zhang, C., Long, D., Li, X., Huang, Q., and Sun, Z.: Generating surface soil moisture at 30 m spatial resolution using both data fusion and machine learning toward better water resources management at the field scale, Remote Sensing of Environment, 255, https://doi.org/ 10.1016/j.rse.2021.112301, 2021.

Acharya, B.S., Dodla, S., Gaston, L.A., Darapuneni, M., Wang, J.J., Sepat, S., and Bohara, H.: Winter cover crops effect on soil moisture and soybean growth and yield under different tillage systems, Soil and Tillage Research, 195, https://doi.org/10.1016/j.still.2019.104430, 2019.

Adams, J.R., McNairn, H., Berg, A.A., and Champagne, C.: Evaluation of near-surface soil moisture data from an AAFC monitoring network in Manitoba, Canada: Implications for L-band satellite validation, Journal of Hydrology, 521, 582-592, https://doi.org/10.1016/j.jhydrol.2014.10.024, 2015.

Al-Yaari, A., Wigneron, J.P., Kerr, Y., Rodriguez-Fernandez, N., O'Neill, P.E., Jackson, T.J., De Lannoy, G.J.M., Al Bitar, A., Mialon, A., Richaume, P., Walker, J.P., Mahmoodi, A., and Yueh, S.: Evaluating soil moisture retrievals from ESA's SMOS and NASA's SMAP brightness temperature datasets, Remote Sensing of Environment, 193, 257-273, https://doi.org/10.1016/j.rse.2017.03.010, 2017.

Bartalis, Z., Wagner, W., Naeimi, V., Hasenauer, S., Scipal, K., Bonekamp, H., Figa, J., and Anderson, C.: Initial soil moisture retrievals from the METOP-A Advanced Scatterometer (ASCAT), Geophysical Research Letters, 34, https://doi.org/10.1029/2007gl031088, 2007.

Beck, H.E., Pan, M., Miralles, D.G., Reichle, R.H., Dorigo, W.A., Hahn, S., Sheffield, J., Karthikeyan, L., Balsamo, G., Parinussa, R.M., van Dijk, A.I.J.M., Du, J., Kimball, J.S., Vergopolan, N., and Wood, E.F.: Evaluation of 18 satellite- and model-based soil moisture products using in situ measurements from 826 sensors, Hydrology and Earth System Sciences, 25, 17-40, https://doi.org/10.5194/hess-25-17-2021, 2021.

Bergstedt, H., Bartsch, A., Duguay, C.R., and Jones, B.M.: Influence of surface water on coarse resolution C-band backscatter: Implications for freeze/thaw retrieval from scatterometer data, Remote Sensing of Environment, 247, 111911, https://doi.org/10.1016/j.rse.2020.111911, 2020.

Breiman, L.: Random forests, Machine Learning, 45, 5-32, https://doi.org/10.1023/A:1010933404324, 2001.

Chan, S.K., Bindlish, R., O'Neill, P., Jackson, T., Njoku, E., Dunbar, S., Chaubell, J., Piepmeier, J., Yueh, S., Entekhabi, D., Colliander, A., Chen, F., Cosh, M.H., Caldwel, T., Walker, J., Berg, A., McNairn, H., Thibeault, M., Martinez-Fernandez, J., Uldall, F., Seyfried, M., Bosch, D., Starks, P., Collins, C.H., Prueger, J., van der Velde, R., Asanuma, J., Palecki, M., Small, E.E., Zreda, M., Calvet, J.C., Crow, W.T., and Kerr, Y.: Development and Assessment of the SMAP Enhanced Passive Soil Moisture Product, Remote Sensing of Environment, 204, 931-941, https://doi.org/10.1016/j.rse.2017.08.025, 2018.

Chan, S.K., Bindlish, R., O'Neill, P.E., Njoku, E., Jackson, T., Colliander, A., Chen, F., Burgin, M., Dunbar, S., Piepmeier, J., Yueh, S., Entekhabi, D., Cosh, M.H., Caldwell, T., Walker, J., Wu, X., Berg, A., Rowlandson, T., Pacheco, A., McNairn, H., Thibeault, M., Martinez-Fernandez, J., Gonzalez-Zamora, A., Seyfried, M., Bosch, D., Starks, P., Goodrich, D., Prueger, J., Palecki, M., Small, E.E., Zreda, M., Calvet, J.-C., Crow, W.T., and Kerr, Y.: Assessment of the SMAP Passive Soil Moisture Product, IEEE Transactions on Geoscience and Remote Sensing, 54, 4994-5007, https://doi.org/10.1109/tgrs.2016.2561938, 2016.

Cho, E., Su, C.-H., Ryu, D., Kim, H., and Choi, M.: Does AMSR2 produce better soil moisture retrievals than AMSR-E over Australia?, Remote Sensing of Environment, 188, 95-105, https://doi.org/10.1016/j.rse.2016.10.050, 2017.

Colliander, A., Jackson, T.J., Bindlish, R., Chan, S., Das, N., Kim, S.B., Cosh, M.H., Dunbar, R.S., Dang, L., Pashaian, L., Asanuma, J., Aida, K., Berg, A., Rowlandson, T., Bosch, D., Caldwell, T., Caylor, K., Goodrich, D., al Jassar, H., Lopez-Baeza, E., Martínez-Fernández, J., González-Zamora, A., Livingston, S., McNairn, H., Pacheco, A., Moghaddam, M., Montzka, C., Notarnicola, C., Niedrist, G., Pellarin, T., Prueger, J., Pulliainen, J., Rautiainen, K., Ramos, J., Seyfried, M., Starks, P., Su, Z., Zeng, Y., van der Velde, R., Thibeault, M., Dorigo, W., Vreugdenhil, M., Walker, J.P., Wu, X., Monerris, A., O'Neill, P.E., Entekhabi, D., Njoku, E.G., and Yueh, S.: Validation of SMAP surface soil moisture products with core validation sites, Remote Sensing of Environment, 191, 215-231, https://doi.org/10.1016/j.rse.2017.01.021, 2017.

Dabrowska-Zielinska, K., Musial, J., Malinska, A., Budzynska, M., Gurdak, R., Kiryla, W., Bartold, M., and Grzybowski, P.: Soil Moisture in the Biebrza Wetlands Retrieved from Sentinel-1 Imagery, Remote Sensing, 10, https://doi.org/10.3390/rs10121979, 2018.

Das, N.N., Entekhabi, D., Njoku, E.G., Shi, J.J.C., Johnson, J.T., and Colliander, A.: Tests of the SMAP Combined Radar and Radiometer Algorithm Using Airborne Field Campaign Observations and Simulated Data, IEEE Transactions on Geoscience and Remote Sensing, 52, 2018-2028, https://doi.org/10.1109/tgrs.2013.2257605, 2014.

De Lannoy, G.J.M., Reichle, R.H., Peng, J., Kerr, Y., Castro, R., Kim, E.J., and Qing, L.: Converting Between SMOS and SMAP Level-1 Brightness Temperature Observations Over Nonfrozen Land, IEEE Geoscience and Remote Sensing Letters, 12, 1908-1912, https://doi.org/10.1109/lgrs.2015.2437612, 2015.

Dorigo, W., Gruber, A., De Jeu, R.A.M., Wagner, W., Stacke, T., Loew, A., Albergel, C., Brocca, L., Chung, D., Parinussa, R.M., and Kidd, R.: Evaluation of the ESA CCI soil moisture product using ground-based observations, Remote Sensing of Environment, 162, 380-395, https://doi.org/10.1016/j.rse.2014.07.023, 2015.

Dorigo, W., Himmelbauer, I., Aberer, D., Schremmer, L., Petrakovic, I., Zappa, L., Preimesberger, W., Xaver, A., Annor, F., Ardö, J., Baldocchi, D., Bitelli, M., Blöschl, G., Bogena, H., Brocca, L., Calvet, J.-C., Camarero, J.J., Capello, G., Choi, M., Cosh, M.C., van de Giesen, N., Hajdu, I., Ikonen, J., Jensen, K.H., Kanniah, K.D., de Kat, I., Kirchengast, G., Kumar Rai, P., Kyrouac, J., Larson, K., Liu, S., Loew, A., Moghaddam, M., Martínez Fernández, J., Mattar Bader, C., Morbidelli, R., Musial, J.P., Osenga, E., Palecki, M.A., Pellarin, T., Petropoulos, G.P., Pfeil, I., Powers, J., Robock, A., Rüdiger, C., Rummel, U., Strobel, M., Su, Z., Sullivan, R., Tagesson, T., Varlagin, A., Vreugdenhil, M., Walker, J., Wen, J., Wenger, F., Wigneron, J.P., Woods, M., Yang, K., Zeng, Y., Zhang, X., Zreda, M., Dietrich, S., Gruber, A., van Oevelen, P., Wagner, W., Scipal, K., Drusch, M., and Sabia, R.: The international soil moisture network: Serving earth system science for over a decade, Hydrology and Earth System Sciences, 25, 5749-5804, https://doi.org/10.5194/hess-25-5749-2021, 2021.

Dorigo, W., Wagner, W., Albergel, C., Albrecht, F., Balsamo, G., Brocca, L., Chung, D., Ertl, M., Forkel, M., Gruber, A., Haas, E., Hamer, P.D., Hirschi, M., Ikonen, J., de Jeu, R., Kidd, R., Lahoz, W., Liu, Y.Y., Miralles, D., Mistelbauer, T., Nicolai-Shaw, N., Parinussa, R., Pratola, C., Reimer, C., van der Schalie, R., Seneviratne, S.I., Smolander, T., and Lecomte, P.: ESA CCI Soil Moisture for improved Earth system understanding: State-of-the art and future directions, Remote Sensing of Environment, 203, 185-215, https://doi.org/10.1016/j.rse.2017.07.001, 2017.

Dorigo, W., Wagner, W., Hohensinn, R., Hahn, S., Paulik, C., Xaver, A., Gruber, A., Drusch, M., Mecklenburg, S., van Oevelen, P., Robock, A., and Jackson, T.: The International Soil Moisture Network: A data hosting facility for global in situ soil moisture measurements, Hydrology and Earth System Sciences, 15, 1675-1698, https://doi.org/10.5194/hess-15-1675-2011, 2011.

El Hajj, M., Baghdadi, N., and Zribi, M.: Comparative analysis of the accuracy of surface soil moisture estimation from the C- and L-bands, International Journal of Applied Earth Observation and Geoinformation, 82, https://doi.org/10.1016/j.jag.2019.05.021, 2019.

Entekhabi, D., Njoku, E.G., O'Neill, P.E., Kellogg, K.H., Crow, W.T., Edelstein, W.N., Entin, J.K., Goodman, S.D., Jackson, T.J., Johnson, J., Kimball, J., Piepmeier, J.R., Koster, R.D., Martin, N., McDonald, K.C., Moghaddam, M., Moran, S., Reichle, R., Shi, J.C., Spencer, M.W., Thurman, S.W., Tsang, L., and Van Zyl, J.: The Soil Moisture Active Passive (SMAP) Mission, Proceedings of the IEEE, 98, 704-716, https://doi.org/ 10.1109/jproc.2010.2043918, 2010.

Escorihuela, M.J., Chanzy, A., Wigneron, J.P., and Kerr, Y.H.: Effective soil moisture sampling depth of L-band radiometry: A case study, Remote Sensing of Environment, 114, 995-1001, https://doi.org/10.1016/j.rse.2009.12.011, 2010.

Fang, B., Kansara, P., Dandridge, C., and Lakshmi, V.: Drought monitoring using high spatial resolution soil moisture data over Australia in 2015–2019, Journal of Hydrology, 594, 125960, https://doi.org/ 10.1016/j.jhydrol.2021.125960, 2021.

Feng, X., Li, J., Cheng, W., Fu, B., Wang, Y., Lü, Y., and Shao, M.: Evaluation of AMSR-E retrieval by detecting soil moisture decrease following massive dryland re-vegetation in the Loess Plateau, China, Remote Sensing of Environment, 196, 253-264, https://doi.org/10.1016/j.rse.2017.05.012, 2017.

Ford, T.W., and Quiring, S.M.: Comparison of contemporary in situ, model, and satellite remote sensing soil moisture with a focus on drought monitoring, Water Resources Research, 55, 1565-1582, https://doi.org/10.1029/2018wr024039, 2019.

https://doi.org/10.5194/essd-2022-137
Preprint. Discussion started: 8 June 2022

Open Access Earth System Science Data Discussions

Grimm, R., Behrens, T., Märker, M., and Elsenbeer, H.: Soil organic carbon concentrations and stocks on Barro Colorado Island — Digital soil mapping using Random Forests analysis, Geoderma, 146, 102-113, https://doi.org/10.1016/j.geoderma.2008.05.008, 2008.

Gruber, A., Dorigo, W.A., Crow, W., and Wagner, W.: Triple Collocation-Based Merging of Satellite Soil moisture Retrievals, IEEE Transactions on Geoscience and Remote Sensing, 55, 6780-6792, https://doi.org/10.1109/tgrs.2017.2734070, 2017.

Gruber, A., Scanlon, T., van der Schalie, R., Wagner, W., and Dorigo, W.: Evolution of the ESA CCI Soil Moisture climate data records and their underlying merging methodology, Earth System Science Data, 11, 717-739, https://doi.org/10.5194/essd-11-717-2019, 2019.

Guillod, B.P., Orlowsky, B., Miralles, D.G., Teuling, A.J., and Seneviratne, S.I.: Reconciling spatial and temporal soil moisture effects on afternoon rainfall, Nat Commun, 6, 6443, https://doi.org/10.1038/ncomms7443, 2015.

Hosseini, M., and McNairn, H.: Using multi-polarization C- and L-band synthetic aperture radar to estimate biomass and soil moisture of wheat fields, International Journal of Applied Earth Observation and Geoinformation, 58, 50-64, https://doi.org/10.1016/j.jag.2017.01.006, 2017.

Hu, F., Wei, Z., Zhang, W., Dorjee, D., and Meng, L.: A spatial downscaling method for SMAP soil moisture through visible and shortwave-infrared remote sensing data, Journal of Hydrology, 590, 125360, https://doi.org/10.1016/j.jhydrol.2020.125360, 2020.

Humphrey, V., Berg, A., Ciais, P., Gentine, P., Jung, M., Reichstein, M., Seneviratne, S.I., and Frankenberg, C.: Soil moisture-atmosphere feedback dominates land carbon uptake variability, Nature, 592, 65-69, https://doi.org/10.1038/s41586-021-03325-5, 2021.

Jaeger, E.B., and Seneviratne, S.I.: Impact of soil moisture–atmosphere coupling on European climate extremes and trends in a regional climate model, Climate Dynamics, 36, 1919-1939, https://doi.org/10.1007/s00382-010-0780-8, 2010.

Jin, Y., Ge, Y., Wang, J., Chen, Y., Heuvelink, G.B.M., and Atkinson, P.M.: Downscaling AMSR-2 Soil Moisture Data With Geographically Weighted Area-to-Area Regression Kriging, IEEE Transactions on Geoscience and Remote Sensing, 56, 2362-2376, https://doi.org/10.1109/tgrs.2017.2778420, 2018.

Kerr, Y.H., Waldteufel, P., Wigneron, J.P., Martinuzzi, J.M., Font, J., and Berger, M.: Soil moisture retrieval from space: The Soil Moisture and Ocean Salinity (SMOS) mission, IEEE Transactions on Geoscience and Remote Sensing, 39, 1729-1735, https://doi.org/Doi 10.1109/36.942551, 2001.

Kim, H., Parinussa, R., Konings, A.G., Wagner, W., Cosh, M.H., Lakshmi, V., Zohaib, M., and Choi, M.: Global-scale assessment and combination of SMAP with ASCAT (active) and AMSR2 (passive) soil moisture products, Remote Sensing of Environment, 204, 260-275, https://doi.org/10.1016/j.rse.2017.10.026, 2018.

Konapala, G., Mishra, A.K., Wada, Y., and Mann, M.E.: Climate change will affect global water availability through compounding changes in seasonal precipitation and evaporation, Nat Commun, 11, 3044, https://doi.org/ 10.1038/s41467-020-16757-w, 2020.

Kumar, S.V., Dirmeyer, P.A., Peters-Lidard, C.D., Bindlish, R., and Bolten, J.: Information theoretic evaluation of satellite soil moisture retrievals, Remote Sensing of Environment, 204, 392-400, https://doi.org/10.1016/j.rse.2017.10.016, 2018.

Larson, K.M., Small, E.E., Gutmann, E.D., Bilich, A.L., Braun, J.J., and Zavorotny, V.U.: Use of GPS receivers as a soil moisture network for water cycle studies, Geophysical Research Letters, 35, https://doi.org/ 10.1029/2008gl036013, 2008.

Li, J., Wang, S., Gunn, G., Joosse, P., and Russell, H.A.J.: A model for downscaling SMOS soil moisture using Sentinel-1 SAR data, International Journal of Applied Earth Observation and Geoinformation, 72, 109-121, https://doi.org/10.1016/j.jag.2018.07.012, 2018.

Liu, Y.Y., Dorigo, W.A., Parinussa, R.M., de Jeu, R.A.M., Wagner, W., McCabe, M.F., Evans, J.P., and van Dijk, A.I.J.M.: Trend-preserving blending of passive and active microwave soil moisture retrievals, Remote Sensing of Environment, 123, 280-297, https://doi.org/10.1016/j.rse.2012.03.014, 2012.

Liu, Y.Y., Parinussa, R.M., Dorigo, W.A., De Jeu, R.A.M., Wagner, W., van Dijk, A.I.J.M., McCabe, M.F., and Evans, J.P.: Developing an improved soil moisture dataset by blending passive and active microwave satellite-based retrievals, Hydrology and Earth System Sciences, 15, 425-436, https://doi.org/ 10.5194/hess-15-425-2011, 2011.

Ma, H., Zeng, J., Chen, N., Zhang, X., Cosh, M.H., and Wang, W.: Satellite surface soil moisture from SMAP, SMOS, AMSR2 and ESA CCI: A comprehensive assessment using global ground-based observations, Remote Sensing of Environment, 231, 111215, https://doi.org/10.1016/j.rse.2019.111215, 2019.

Ma, S., Zhang, S., Wang, N., Huang, C., and Wang, X.: Prolonged duration and increased severity of agricultural droughts during 1978 to 2016 detected by ESA CCI SM in the humid Yunnan Province, Southwest China, Catena, 198, 105036, https://doi.org/10.1016/j.catena.2020.105036, 2021.

McNally, A., Shukla, S., Arsenault, K.R., Wang, S., Peters-Lidard, C.D., and Verdin, J.P.: Evaluating ESA CCI soil moisture in East Africa, Int J Appl Earth Obs Geoinf, 48, 96-109, https://doi.org/10.1016/j.jag.2016.01.001, 2016.

Meng, X., Bao, Y., Liu, J., Liu, H., Zhang, X., Zhang, Y., Wang, P., Tang, H., and Kong, F.: Regional soil organic carbon prediction model based on a discrete wavelet analysis of hyperspectral satellite data, International Journal of Applied Earth Observation and Geoinformation, 89, 102111, https://doi.org/10.1016/j.jag.2020.102111, 2020.

Njoku, E.G., Jackson, T.J., Lakshmi, V., Chan, T.K., and Nghiem, S.V.: Soil moisture retrieval from AMSR-E, IEEE Transactions on Geoscience and Remote Sensing, 41, 215-229, https://doi.org/10.1109/tgrs.2002.808243, 2003.

Njoku, E.G., Wilson, W.J., Yueh, S.H., Dinardo, S.J., Li, F.K., Jackson, T.J., Lakshmi, V., and Bolten, J.: Observations of soil moisture using a passive and active low-frequency microwave airborne sensor during SGP99, IEEE Transactions on Geoscience and Remote Sensing, 40, 2659-2673, https://doi.org/10.1109/tgrs.2002.807008, 2002.

Owe, M., de Jeu, R., and Holmes, T.: Multisensor historical climatology of satellite-derived global land surface moisture, Journal of Geophysical Research, 113, https://doi.org/10.1029/2007jf000769, 2008.

Pascolini-Campbell, M., Reager, J.T., Chandanpurkar, H.A., and Rodell, M.: A 10 per cent increase in global land evapotranspiration from 2003 to 2019, Nature, 593, 543-547, https://doi.org/ 10.1038/s41586-021-03503-5, 2021.

Peng, J., Loew, A., Merlin, O., and Verhoest, N.E.C.: A review of spatial downscaling of satellite remotely sensed soil moisture, Reviews of Geophysics, 55, 341-366, https://doi.org/10.1002/2016rg000543, 2017.

Piles, M., Camps, A., Vall-llossera, M., Corbella, I., Panciera, R., Rudiger, C., Kerr, Y.H., and Walker, J.: Downscaling SMOS-Derived Soil Moisture Using MODIS Visible/Infrared Data, IEEE Transactions on Geoscience and Remote Sensing, 49, 3156-3166, https://doi.org/10.1109/tgrs.2011.2120615, 2011.

Piles, M., Entekhabi, D., and Camps, A.: A Change Detection Algorithm for Retrieving High-Resolution Soil Moisture from SMAP Radar and Radiometer Observations, IEEE Transactions on Geoscience and Remote Sensing, 47, 4125-4131, https://doi.org/10.1109/tgrs.2009.2022088, 2009.

Raju, S., Chanzy, A., Wigneron, J.P., Calvet, J.C., Kerr, Y., and Laguerre, L.: Soil-Moisture and Temperature Profile Effects on Microwave Emission at Low-Frequencies, Remote Sensing of Environment, 54, 85-97, https://doi.org/ Doi 10.1016/0034-4257(95)00133-L, 1995.

Rigden, A.J., Mueller, N.D., Holbrook, N.M., Pillai, N., and Huybers, P.: Combined influence of soil moisture and atmospheric evaporative demand is important for accurately predicting US maize yields, Nature Food, 1, 127-133, https://doi.org/10.1038/s43016-020-0028-7, 2020.

https://doi.org/10.5194/essd-2022-137
Preprint. Discussion started: 8 June 2022

Open Access Earth System Science Data Discussions

Wang, X., Lü, H., Crow, W.T., Zhu, Y., Wang, Q., Su, J., Zheng, J., and Gou, Q.: Assessment of SMOS and SMAP soil moisture products against new estimates combining physical model, a statistical model, and in-situ observations: A case study over the Huai River Basin, China, Journal of Hydrology, 598, 126468, https://doi.org/10.1016/j.jhydrol.2021.126468, 2021.

Wood, E.F., Sheffield, J., Schlosser, C.A., Robertson, F.R., Liu, W.T., Lettenmaier, D.P., Huffman, G.J., Hilburn, K., Gu, G., Gao, X., Fetzer, E.J., Clark, E., Chambers, D., Clayson, C.A., Bosilovich, M.G., Adler, R., Houser, P.R., Famiglietti, J.S., Olson, W.S., L'Ecuyer, T.S., Beaudoing, H.K., and Rodell, M.: The Observed State of the Water Cycle in the Early Twenty-First Century, Journal of Climate, 28, 8289-8318, https://doi.org/ 10.1175/jcli-d-14-00555.1, 2015.

Wu, M., Scholze, M., Kaminski, T., Voßbeck, M., and Tagesson, T.: Using SMOS soil moisture data combining CO2 flask samples to constrain carbon fluxes during 2010–2015 within a Carbon Cycle Data Assimilation System (CCDAS), Remote Sensing of Environment, 240, 111719, https://doi.org/10.1016/j.rse.2020.111719, 2020.

Yang, H., Wang, Q., Zhao, W., and Atkinson, P.M., An 8-day composited 36 km SMAP soil moisture dataset (1979-2015), Figshare, https://doi.org/10.6084/m9.figshare.17621765, 2021.

Zhang, R., Kim, S., Sharma, A., and Lakshmi, V.: Identifying relative strengths of SMAP, SMOS-IC, and ASCAT to capture temporal variability, Remote Sensing of Environment, 252, 112126, https://doi.org/ 10.1016/j.rse.2020.112126, 2021.

Zhao, B., Dai, Q., Zhuo, L., Zhu, S., Shen, Q., and Han, D.: Assessing the potential of different satellite soil moisture products in landslide hazard assessment, Remote Sensing of Environment, 264, 112583, https://doi.org/ 10.1016/j.rse.2021.112583, 2021.

Zhao, W., Sánchez, N., Lu, H., and Li, A.: A spatial downscaling approach for the SMAP passive surface soil moisture product using random forest regression, Journal of Hydrology, 563, 1009-1024, https://doi.org/10.1016/j.jhydrol.2018.06.081, 2018.

Zhou, S., Williams, A.P., Lintner, B.R., Berg, A.M., Zhang, Y., Keenan, T.F., Cook, B.I., Hagemann, S., Seneviratne, S.I., and Gentine, P.: Soil moisture–atmosphere feedbacks mitigate declining water availability in drylands, Nature Climate Change, 11, 38-44, https://doi.org/10.1038/s41558-020-00945-z, 2021.

Zhou, Y., Xiao, X., Zhang, G., Wagle, P., Bajgain, R., Dong, J., Jin, C., Basara, J.B., Anderson, M.C., Hain, C., and Otkin, J.A.: Quantifying agricultural drought in tallgrass prairie region in the U.S. Southern Great Plains through analysis of a water-related vegetation index from MODIS images, Agricultural and Forest Meteorology, 246, 111-122, https://doi.org/10.1016/j.agrformet.2017.06.007, 2017.